Journal of Atmospheric and Solar-Terrestrial Physics 73 (2011) 335–347

Contents lists available at ScienceDirect

Journal of Atmospheric and Solar-Terrestrial Physics

journal homepage: www.elsevier.com/locate/jastp

Recalibration of the long-term NOAA/MEPED energetic proton measurements

T. Asikainen *, K. Mursula

Department of Physics, Centre of Excellence in Research, University of Oulu, P.O. Box 3000, FIN-90014, Finland

ARTICLE INFO

Article history:
Accepted 28 December 2009
Available online 6 January 2010

Keywords:
NOAA
MEPED
Correction of data
Radiation damage

ABSTRACT

The MEPED instruments onboard the low-altitude polar orbiting NOAA/POES satellites have measured energetic particles since 1978, offering a nearly continuous series of energetic particle fluxes in the magnetosphere during three solar cycles. However, there are several problems in using these data for long-term studies, the most significant one being that the solid state detectors of the MEPED proton instruments suffer significant radiation damage. This causes the effective energy thresholds of the instrument to increase, leading to underestimated particle fluxes already a couple of years after satellite launch. Before the MEPED data can reliably be used in any long-term study the data have to be recalibrated taking into account the decay of the detectors. In this paper we present quantified estimates of the degree of radiation damage for all NOAA/POES satellites, a method for correcting the MEPED proton measurements, and give an estimate of energetic proton fluxes from 1978 to present.

1. Introduction

The long-term variation of the Sun and its effects in the magnetosphere-ionosphere-atmosphere system are of considerable interest. One of the longest nearly continuous datasets of magnetospheric energetic particle measurements has been obtained by the NOAA/POES (Polar Orbiting Environmental Satellites) program which has been operational since 1978, i.e., already for three solar cycles. The satellite program consists of a number of low-altitude polar satellites whose versatile instrument set is designed to monitor the Earth, its atmosphere and space environment. The NOAA energetic particle dataset has been used for decades, e.g., in studying the particle precipitation in auroral zones (e.g. Wissing et al., 2008), constructing radiation belt models (e.g. Fung, 1996; Huston et al., 1996), studying magnetic storm dynamics (Søraas et al., 2002, 2004; Asikainen et al., 2005) and studying the South Atlantic Anomaly and inner radiation belts (Asikainen and Mursula, 2005, 2008). Accordingly, the continually expanding NOAA/POES dataset has established itself as one of the most important long-term energetic particle datasets in space physics.

However, nearly a decade ago, it was noticed that the energetic particle measurements by NOAA/MEPED proton detectors showed clear signs of instrument degradation due to radiation damage that leads to erroneous fluxes and artificial long-term trends in the data (Galand and Evans, 2000; McFadden et al., 2007). The signs of radiation damage typically became significant a couple of years after satellite launch. The data in the beginning of the operational period of each satellite are fairly reliable (with the exception of NOAA-14 whose MEPED instrument showed erroneous fluxes from the beginning of the mission). However, after this time interval, especially in view of long-term studies covering one solar cycle or more, the data can no longer be trusted. Although the instrument degradation has been known for quite some time there are so far no systematic documented attempts to correct the measurements. We have studied the effects of radiation damage to the NOAA/MEPED proton detectors in detail and report in this paper a method to fairly reliably correct the degraded data.

The paper is organized as follows. We will first review the basic properties of the NOAA satellites and the MEPED instrument in Section 2. In Section 3 we explain the physical model of radiation damage upon which our correction method is based. In Section 4 we describe how we can assess the level of degradation by comparing an earlier satellite with a newly launched satellite that has not yet degraded. In Section 5 we discuss the time evolution of the instrument degradation. In Section 6 we present the corrected proton measurements for all NOAA/POES satellites and compare them with the uncorrected data. The conclusions are given in the last section.

2. POES satellites and MEPED instruments

The NOAA/POES (Polar Orbiting Environmental Satellites) program was started in 1978 as the TIROS-N satellite was launched. Since then several satellites have been launched to replace and supplement the older satellites. The time coverages of

* Corresponding author. Tel.: +358 8 553 1302.
E-mail address: timo.asikainen@oulu.fi (T. Asikainen).

1364-6826/$ - see front matter © 2010 Elsevier Ltd. All rights reserved.
doi:10.1016/j.jastp.2009.12.011

NOAA satellites that have measured energetic particles are given in Table 1 and depicted in Fig. 1 with a reference to solar cycles. The POES satellites orbit the Earth on nearly circular, Sun sychronous, polar orbits with a nominal altitude of about 850 km and an orbital period of about 102 min. The orbital planes relative to the Sun-Earth line stay relatively constant ('Sun synchronous') although over a period of several years the orientation of the orbital planes rotates significantly. E.g., NOAA-16 orbital plane in 2001 was post-midnight–afternoon but currently in 2009 it has rotated to the dawn-dusk plane.

The NOAA satellites include a SEM (Space Environment Monitor) instrument package that consists of two separate instruments for measuring charged particles; TED (Total Energy Detector) and MEPED (Medium Energy Proton Electron Detector). The satellites up to NOAA-14 had the SEM-1 version of the instrument while starting from NOAA-15 the satellites carry an improved version of the instrument called SEM-2. The TED instrument measures lower energy auroral particle fluxes below 20 keV energy and MEPED, in which we concentrated here, measures higher energy particles. MEPED consists of two separate detectors that measure energetic electrons at nominal energy range 30 keV–2.5 MeV in three integral energy channels, and energetic protons at nominal energy range from 30 keV upwards in six differential energy channels (in the older SEM-1 package MEPED had only five differential proton channels). The nominal energy ranges of the electron (E) and proton (P) detector channels for protons and electrons (for SEM-2 and SEM-1) are given in Table 2. No charge/mass separation is implemented in MEPED so the proton detector also measures heavier ions. It also has some sensitivity mostly in the highest P6 channel (in SEM-2, P5 channel in SEM-1) to relativistic electrons above 800 keV which cannot be stopped by the magnet shielding the aperture of the MEPED proton detector (instrument builder estimated this to be about 30% of incoming relativistic electrons). The sensitivity of P1–P3 channels to energetic electrons is negligibly small and P4–P5 (in SEM-2, P4 in SEM-1) are not sensitive to electrons at all. Furthermore the electron detector is sensitive to protons of certain energies (see Table 2) with an efficiency of 100%.

The MEPED protons and electrons are measured in two nearly orthogonal directions with a sampling time of 2 s. In SEM-2 the local vertical detector, the so called 0° detector points away from the Earth along the radial Earth-satellite line (towards $-X$ axis in satellite coordinates) and the local horizontal detector, the so called 90° detector points antiparallel to spacecraft velocity vector (towards $+Y$ axis of the satellite coordinate system). To ensure a clear field of view the 0° detector has been rotated 9° from $-X$ axis towards the $-Z$ axis and the 90° detector has been rotated 9° from $+Y$ towards $-Z$ axis. (However, in METOP-02 the detectors point directly towards $-X$ and $+Y$ axes respectively). This orientation of the detectors means that at high latitudes where the magnetic field lines near the Earth are nearly radial the 0° detector measures field aligned precipitating particles and the 90° detector measures locally trapped particles. At low latitudes the situation is different so that the 90° measures field-aligned particles (either precipitating or upflowing, depending on the direction of satellite motion and the hemisphere) and 0° measures locally trapped particles. In SEM-1 the 0° detector is pointed in the same direction as in SEM-2. The 90° detector, however, is approximately pointed towards the $-Z$ axis from where it has been rotated 9° towards $-X$

Table 1
Time coverage of NOAA POES satellite measurements.

Satellite	Time coverage of measurements
TIROS-N	02 November 1978–28 February 1981
NOAA-06	27 June 1979–21 November 1986
NOAA-07	07 November 1981–10 February 1985
NOAA-08	01 May 1983-21 October 1985
NOAA-10	21 October 1986–31 August 1991
NOAA-12	01 June 1991–30 December 2001
NOAA-14	11 January 1995–31 December 2004
NOAA-15	01 July 1998–present
NOAA-16	01 October 2001–present
NOAA-17	12 July 2002–present
NOAA-18	07 June 2005–present
METOP-02	12 March 2006–present
NOAA-19	23 February 2009–present

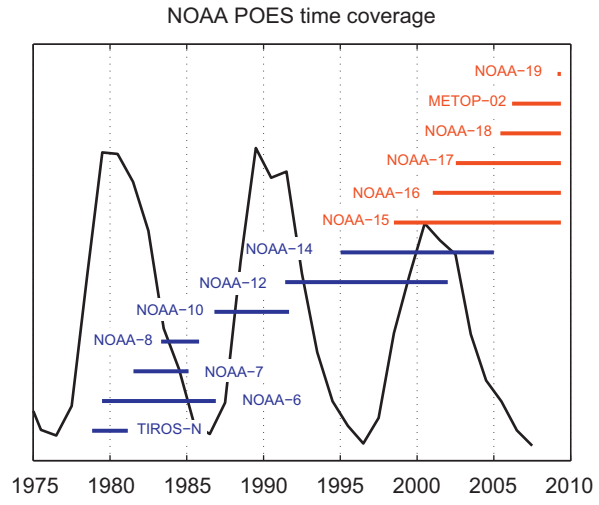

Fig. 1. Time coverage of NOAA POES satellites with the sunspot cycle shown as a reference. The satellites coded as blue (black in grayscale) represent the older SEM-1 energetic particle instruments while the newer satellites having SEM-2 instruments are coded red (gray in grayscale). (For interpretation of the references to color in this figure legend, the reader is referred to the web version of this article.)

Table 2
Nominal energy ranges of the MEPED SEM-2 instrument.

Energy channel	Nominal energy range of protons (keV)	Nominal energy range of contaminating electrons (keV)
P1	30–80	–
P2	80–240 (80–250 for SEM-1)	–
P3	240–800 (250–800 for SEM-1)	–
P4	800–2500	–
P5	2500–6900	$-(\gtrsim 800$[a] for SEM-1)
P6	>6900 (no P6 in SEM-1)	$\gtrsim 800$[a]
Energy channel	**Nominal energy range of electrons**	**Nominal energy range of contaminating protons (keV)**
E1	30–2500	210–2700
E2	100–2500	280–2700
E3	300–2500	440–2700

The energy ranges for SEM-1 version of the instrument are the same except when indicated otherwise.
The P-channels refer to proton detector and E-channels to electron detector. Both detectors are sensitive to both particle species to some degree. The proton counting efficiency of the electron channels is 100%.

[a] The nominal electron counting efficiency of P6 (SEM-2, P5 in SEM-1) channel is estimated by the instrument builder to be about 30% of incoming relativistic electrons. The sensitivity of P1–P3 channels to energetic electrons is negligibly small and P4–P5 (P4 in SEM-1) are not sensitive to electrons at all.

axis to ensure a clear field of view. The measured count rates (particles/sec) are converted to physical fluxes (particles/cm^2 sr s) by dividing with the geometric factor G of the detector. For SEM-1 the geometric factor is $G = 0.0095\,\mathrm{cm}^2\,\mathrm{sr}$ and for SEM-2 $G = 0.01\,\mathrm{cm}^2\,\mathrm{sr}$. A more detailed description of the SEM-1 and SEM-2 instruments is given by Hill et al. (1985), Seale and Bushnell (1987), Raben et al. (1995) and Evans and Greer (2000), respectively.

3. Effects of the radiation damage on MEPED

The MEPED electron and proton detectors are typical solid state silicon detectors based on pulse-height analysis. In such a detector a charged particle penetrating the detector chip loses some or all of its kinetic energy and produces free charge carriers (electrons and holes) in the silicon lattice. The number of produced free charges is directly proportional to the kinetic energy lost by the incoming particle. The detector electronics then collects the charge produced in the silicon chip within some integration time (85 ns in MEPED) and the charge is then transformed to a voltage pulse whose amplitude is recorded. This pulse amplitude is a measure of the kinetic energy of the incoming particle. By counting the number of pulses and their heights each second (a full data readout from both 0° and 90° detectors takes 2 s since the counting electronics is shared between the detectors) MEPED obtains the energy distribution of incoming particles which then can be used to sort particles into respective energy channels with specific thresholds given in Table 2.

It is a well known fact that the silicon detectors in general are prone to radiation damage caused by the incoming energetic particles and ionizing electromagnetic radiation (see e.g., Grupen and Shwartz, 2008). To minimize the effects of solar radiation the MEPED detectors are covered with a thin metal film (aluminum in proton detectors and nickel in electron detectors) that stops most of the harmful electromagnetic radiation but still allows particles to penetrate into the detectors. Accordingly, the radiation damage of the MEPED instrument is caused by the very same particles that it measures. The incomimg particles create defects in the silicon lattice that reduce the mobility of the free charge carriers. Consequently, the amount of charge collected during the instrument integration time is reduced and thus the energy of the incoming particle is underestimated. Accordingly, as radiation damage progresses particles need more and more energy to be detected in a given channel. In the present analysis below we denote by α_i the factors by which lower energy threshold of the i th energy channel has increased from the nominal values given in Table 2. It is important to note that the α factors are not constant but change in time.

4. Recalibration method

4.1. Satellite conjunctions

The goal of the recalibration is to estimate the α factors by which the energy thresholds have increased in time, and their temporal evolution and then use the α factors to correct the measured fluxes. In order to estimate the α factors we also need to know the true particle spectrum that an undegraded MEPED instrument would measure in order to compare that to the measurements by the degraded instrument. We have compared the measurements by an earlier, degraded NOAA satellite to a newly launched satellite whose instruments have not yet suffered significant radiation damage. Such a comparison is possible only soon after the launch of a new POES satellite (see Fig. 1). To have a truthful comparison, the two satellites have to sample the same region of space as closely as possible and as simultaneously as possible. We have thus studied the conjunctions between any two satellites using the following criteria:

1. The conjunction must be within five month from the launch of the new satellite (this time interval was chosen as a compromise between obtaining enough conjunctions on one hand and maintaining low level of radiation damage in the newly launched satellite on the other hand);
2. The latitudinal and longitudinal difference (in geomagnetic coordinates) of the footpoints (at 120 km altitude) of the magnetic field lines confining the two satellites must be $< 1^\circ$;
3. The relative difference in the L-values of the satellites must be $< 10\%$;
4. The particle count rates at the lowest energy channels must exceed the one count level;
5. The time difference between two conjugate measurements (as defined by the above conditions) must be < 30 s.

Since the satellite orbits are polar the conjunctions occur mostly at very high latitudes, often within the polar cap, where energetic particle fluxes are typically very low. Fortunately still, many conjunctions occurred around the auroral zone and in the outer radiation belt where significant particle fluxes were detected. One conjunction typically consisted of a few tens of 2 s measurements from both satellites. Each measurement of one satellite is spatially and temporally in conjunction with at least one measurement of the other satellite. We compare each pair of conjugating measurements (e.g., 10 data points from one satellite all in conjunction with 10 datapoints from the other satellite would yield $10 \times 10 = 100$ comparisons). Furthermore, we have typically tens of conjunctions for each satellite pair, which leads to hundreds of comparisons between two satellites each time a new satellite is launched. Table 3 presents the number of conjunctions for each pair of satellites. The columns represent the degraded satellites and the rows the newly launched satellites so that, e.g., for NOAA-15 and NOAA-16 a total of 31 separate conjunctions was found soon after NOAA-16 launch. Note that since NOAA-07 and NOAA-08 do not have any conjunctions we cannot determine their α factors. However, since these satellites did not actively produce measurements for more than a few years the effect of radiation damage can be assumed to be minimal. We also note that unfortunately NOAA-06 and NOAA-10 did not have

Table 3
Number of conjunctions between each pair of satellites.

	Old satellite				
New satellite	NOAA-06	NOAA-07	NOAA-08	NOAA-10	NOAA-12
NOAA-07	5	–	–	–	–
NOAA-08	–	–	–	–	–
NOAA-10	–	–	–	–	–
NOAA-12	–	–	–	6	–
NOAA-15	–	–	–	–	6
New satellite	**NOAA-15**	**NOAA-16**	**NOAA-17**	**NOAA-18**	**METOP-02**
NOAA-16	31	–	–	–	–
NOAA-17	33	50	–	–	–
NOAA-18	18	50	56	–	–
METOP-02	22	30	17	25	–
NOAA-19	11	9	17	0	31

The columns represent the degraded satellites and the rows column the newly launched satellites.

any conjunctions since the NOAA-06 measurements end in 5 March 1986, about 7 month before the start of NOAA-10 measurements in 11 October 1986. Due to this, the series of corrected measurements will not be continuous. The problem arising from this discontinuity is discussed and solved later on in the paper.

4.2. Determining the α factors

Let us now compare the measurements of two satellites in detail, and the estimate the α factors. Let the integral proton energy spectrum measured by the newly launched satellite be

$$F_n(E) = \int_E^{\infty} f_n(E')\,dE', \tag{1}$$

where the index n refers to 'new' satellite and $f_n(E)$ would be the differential energy spectrum i.e., $F_n(E)$ is the flux of protons observed above energy E. We assume that $F_n(E)$ is the true integral spectrum that should be sampled by both satellites. If we now assume that in the degraded satellite the energy threshold of the i th channel has increased by a factor of α_i we can express the measured integral flux above energy $\alpha_i E_i$ as

$$F_n(\alpha_i E_i) = \frac{1}{G_o}\sum_{k=i}^{k=5} N_{o,k}, \tag{2}$$

where the index o refers to 'old' satellite and $N_{o,k}$ is the count rate measured by the degraded old satellite at channel k and G_o is the geometric factor of the instrument which converts the count rate to flux (see Section 2). Note that Eq. (2) holds only for protons up to the 5th energy channel. We have dropped the 6th energy channel from our α factor analysis to avoid issues arising from the contamination of this channel by relativistic electrons. Omitting the P6 channel has minor effect on the analysis since P6 count rates are always much lower than other channels when relativistic electrons are not present.

Before we can solve α_i from Eq. (2) we need to determine the integral spectrum $F_n(E)$. We obtain a numerical representation of the integral spectrum $F_n(E)$ by fitting a monotonic piecewise cubic hermite interpolating polynomial (PCHIP) to the measurements of the newly launched satellite. Such a polynomial is the most suitable interpolant for this situation since it maintains the monotonicity of the spectrum at all points and its derivative is continuous (for more detailed information on PCHIP polynomials see e.g. Fritsch and Carlson, 1980). We do the fitting in logarithmic scale using X_i and Y_i values given by

$$X_i = \log E_i, \tag{3}$$

$$Y_i = \log\left(\frac{1}{G_n}\sum_{k=i}^{k=5} N_{n,k}\right), \tag{4}$$

where E_i is the nominal lower energy threshold of the i th energy channel, G_n the geometric factor of the new satellite and $N_{n,k}$ is the proton count rate at k th channel measured by the newly launched satellite. If the integral count rate in some channel is zero (as it is in many cases) we have assigned the count rate a value of 0.1, which is below the one count level. In case the count rates at all channels are zero all integral count rates are given the value of 0.1. This does not affect the results but allows us to calculate the logarithmic Y_i values. After determining the interpolant we can solve Eq. (2) numerically and obtain the α_i factors for different energy channels. Fig. 2 shows graphically how the α factors are determined by finding the energy in the spectrum of the new satellite where the fluxes match those of the old satellite. The depicted spectra are samples of real measurements.

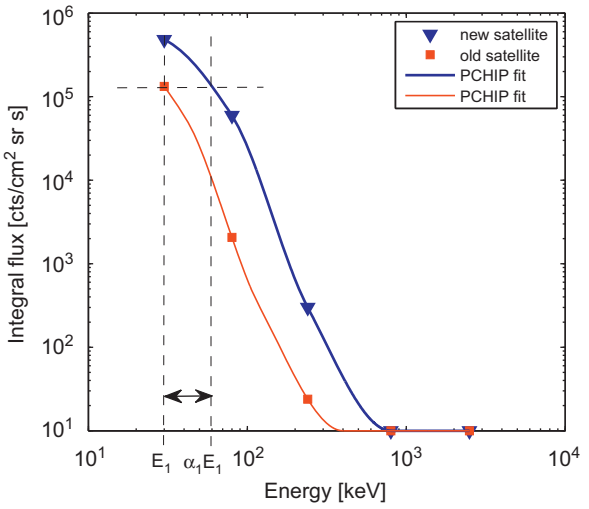

Fig. 2. A schematic picture depicting the determination of the α factors. The blue (black in grayscale) triangles show the integral count rates measured by a new satellite and the red (gray in grayscale) squares show the same for an old satellite. The curves are PCHIP interpolants in the logarithmic scale. The α factors are determined by finding the energy in the spectrum of the new satellite where the counts match those of the old satellite. (For interpretation of the references to color in this figure legend, the reader is referred to the web version of this article.)

As mentioned above, when comparing the data between two satellites we obtain tens of α factors for each conjunction (and we have several conjunctions per satellite pair). Since the conjunctions between the satellites are not exact spatially or temporally the distributions of α factors contain some statistical variation around the average value. To obtain the final α factors we take as α the median of the distribution. As the measure of error we take the median absolute deviation (MAD) of the distribution, which is defined as

$$\mathrm{MAD}(\alpha) = \mathrm{median}(|\alpha - \mathrm{median}(\alpha)|).$$

These statistics are more robust than mean or standard deviation which are more sensitive to outliers. An example of α−factor histograms obtained for NOAA-15 and NOAA-18 in 2005 soon after NOAA-18 launch is shown in Fig. 3. The distribution of α values is given for the three lowest energy channels of the 0° detector. The α distributions closely resemble the log-normal distribution with a fairly well defined mean and standard deviation. The distributions sometimes show anomalous spikes (like in the P2-channel distrubution in Fig. 3) arising from situations where the numerical solution of Eq. (2) does not converge. Such anomalous values are robustly disregarded by computing the median and MAD values as explained above.

4.3. Correcting the count rates

After the α factors of the different energy channels have been determined we can use them to calculate the corrected count rates at each nominal energy channel i.e., we calculate what the count rate of the degraded satellite would be if the energy thresholds were still the same as the nominal thresholds in Table 2. The correction of the count rates is based on computing the count rates at the nominal energies from the spectrum based on measurements at the increased energy thresholds. For this purpose a fit must be made to the observed spectrum. Since the spectral shape in general is not known and evidently varies from measurement to another, we have used the PCHIP interpolant to construct the integral spectrum of the old degraded satellite. (We note that in cases where the spectral shape is more accurately known a better fit to the spectrum might be obtained by different

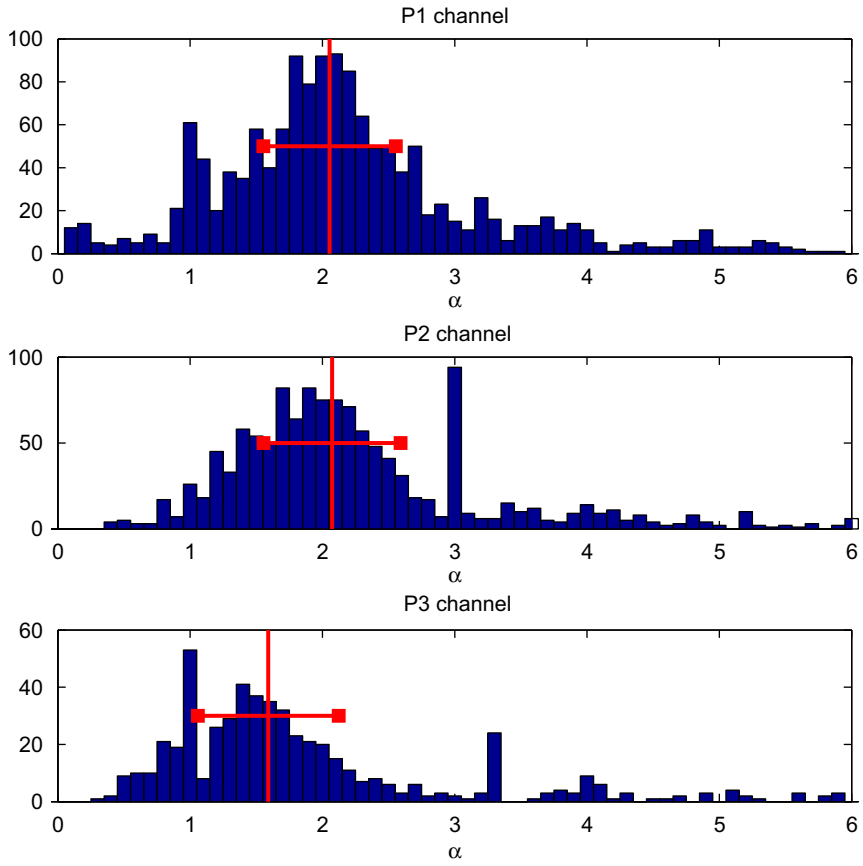

Fig. 3. An example of the α−factor histograms obtained by comparing NOAA-15 and NOAA-18 in 2005 soon after NOAA-18 launch. The distribution of α values are given for the three lowest energy channels of the 0° detector. The red (gray in grayscale) vertical lines show the median of the distributions and the horizontal lines show the MAD values around the medians. (For interpretation of the references to color in this figure legend, the reader is referred to the web version of this article.)

methods.) We compute the PCHIP interpolant in logarithmic scale using the values given by

$$X_i = \log(\alpha_i E_i), \tag{5}$$

$$Y_i = \log\left(\sum_{k=i}^{k=5} N_{o,k}\right). \tag{6}$$

We can then calculate the corrected count rate $N_{c,i}$ at the i th energy channel from the following equation

$$N_{c,i} = F_o(E_i) - F_o(E_{i+1}), \tag{7}$$

where $F_o(E)$ is the PCHIP interpolant of the degraded satellite and $i = 2, 3, 4, 5$ (for $\mathbf{i = 5}$ $\mathbf{F_o(E_6)}$ is assumed to be negligibly small). These corrected counts based on the PCHIP interpolant are rather reliable only above energy $\alpha_1 E_1$, i.e., the lowest energy channel. Correcting the counts of the lowest energy channel (and the second energy channel if α_1 is sufficiently high) requires extrapolating the spectrum to lower energies than measured by the degraded instrument. Extrapolation is inherently less accurate than interpolation and the error related to the extrapolation is expected to grow with the α factors. Choosing a suitable extrapolation method for the correction of the lowest energy channel is important but not trivial. First we used linear extrapolation in logaritmic scale. However, this is not expected to yield a very good result since the measured spectrum exhibits nearly always some degree of curvature in the logarithmic scale (see for example Fig. 2). Due to curvature the linear extrapolation will either overestimate the count rates (if the spectrum curves down) or underestimate them (if the spectrum curves up). Extrapolation is needed whenever the lowest energy ($\alpha_1 E_1$) of the degraded satellite exceeds the nominal energy of the channel we are correcting, i.e., if $\alpha_1 E_1 > E_i$ (mostly this affects only the lowest energy channel but when $\alpha_1 > 2.667$ the second energy channel also requires extrapolation). For the lowest energy channel we extrapolate by fitting a line to the count rates (measured by the degraded satellite) at the energy $\alpha_1 E_1$ and the corrected second energy channel at energy E_2. Generalizing, for i th energy channel requiring extrapolation this method leads to the following expression

$$N_{c,i} = \exp\left[\log N_{o,i} - \frac{\log\left(\frac{N_{c,i+1}}{N_{o,i}}\right)}{\log\left(\frac{E_{i+1}}{\alpha_i E_i}\right)} \log\alpha_i\right]. \tag{8}$$

As will be shown later linear extrapolation tends to overestimate the fluxes especially when α−factor of the channel is large ($\gtrsim 1.5$). Therefore, we have also used another method of extrapolation by fitting the integral of the Maxwellian spectrum to the two lowest energy channels and then extrapolating downwards in energy. It can be shown that the integral spectrum (as defined in Eq. (1)) for a Maxwellian distribution

$$f_{Max}(E) = \frac{2n}{\sqrt{\pi}} \sqrt{\frac{E}{E_0^3}} \exp\left(-\frac{E}{E_0}\right) \tag{9}$$

is

$$F_{Max}(E, E_0) = n\left(1 - \mathrm{erf}\sqrt{\frac{E}{E_0}}\right) + \frac{2n}{\sqrt{\pi}} \sqrt{\frac{E}{E_0}} \exp\left(-\frac{E}{E_0}\right), \tag{10}$$

where n is the total particle count over all energies and $E_0 = kT$ is the average thermal energy of the particles. The parameter E_0 can

be solved numerically from the following equation:

$$\frac{\sum_{k=1}^{k=5} N_{o,k}}{\sum_{k=2}^{k=5} N_{o,k}} = \frac{F_{Max}(\alpha_1 E_1, E_0)}{F_{Max}(\alpha_2 E_2, E_0)}, \quad (11)$$

where the sums at the numerator and the denominator represent the integral count rates at channels P1 and P2 respectively. The total particle count n can then be obtained from

$$n = \frac{N_1}{F_{Max}(\alpha_1 E_1, E_0)}. \quad (12)$$

Finally, the corrected count rate of the first energy channel is (in this approach, similarly for the second channel if needed)

$$N_{c,1} = F_{Max}(E_1, E_0) - F_o(E_2), \quad (13)$$

where the latter integral spectrum $F_o(E)$ is the PCHIP interpolant of the degraded satellite. Note that if $E_0 \gg \alpha_1 E_1$ the Maxwellian spectrum below $\alpha_1 E_1$ is almost flat. In this case we have used simple linear extrapolation in logarithmic scale as described above in order to speed up the computations.

5. Time evolution of MEPED degradation

Figs. 4–11 show the α–factors as a function of time for the three lowest energy channels for all those NOAA satellites for which the determination of the factors was possible. At higher energy channels the count rates during conjunctions were too low to permit a reliable estimation of the α–factors. This was also the case for the 2nd and 3rd energy channels of NOAA-12 (see Fig. 6), where the degradation of the instrument had progressed so far (conjunction with NOAA-15 occurred about 10 years after NOAA-12 launch) that significant count rates could not be obtained

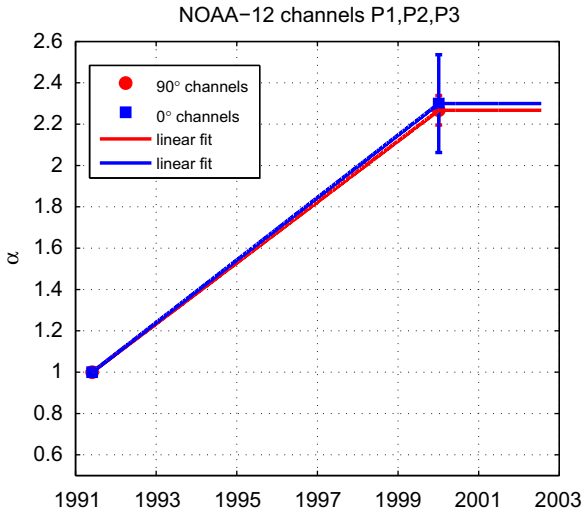

Fig. 6. The α factors of NOAA-12 as a function of time for the three lowest energy channels. The blue (black in grayscale) squares depict the 0° channel and the red (gray in grayscale) circles the 90° channel. Due to the lack of significant count rates of P2 and P3 channels during conjunctions, the α–factors at these channels were assigned the same value as the P1 channel. The α factors are based on conjunctions between NOAA-12 and NOAA-15. (For interpretation of the references to color in this figure legend, the reader is referred to the web version of this article.)

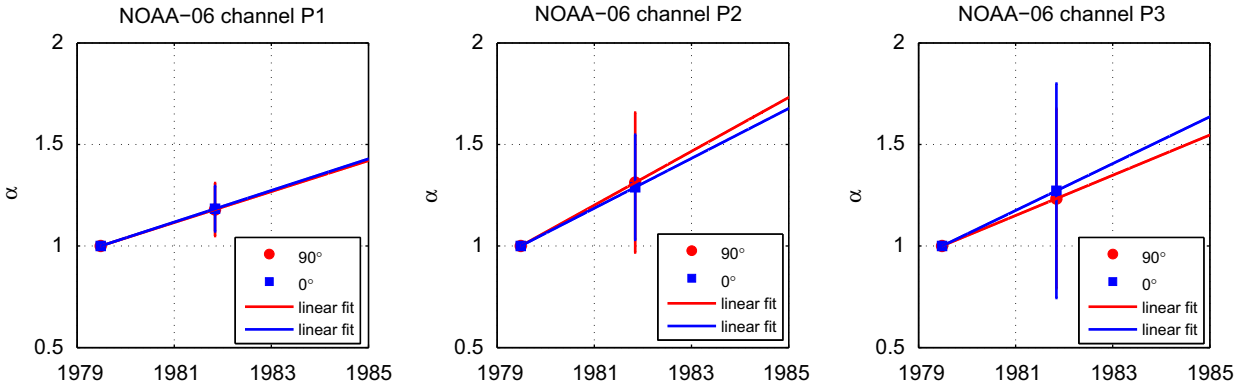

Fig. 4. The α factors of NOAA-06 as a function of time for the three lowest energy channels. The blue (black in grayscale) squares depict the 0° channel and the red (gray in grayscale) circles the 90° channel. The α factors are based on conjunctions between NOAA-06 and NOAA-07. (For interpretation of the references to color in this figure legend, the reader is referred to the web version of this article.)

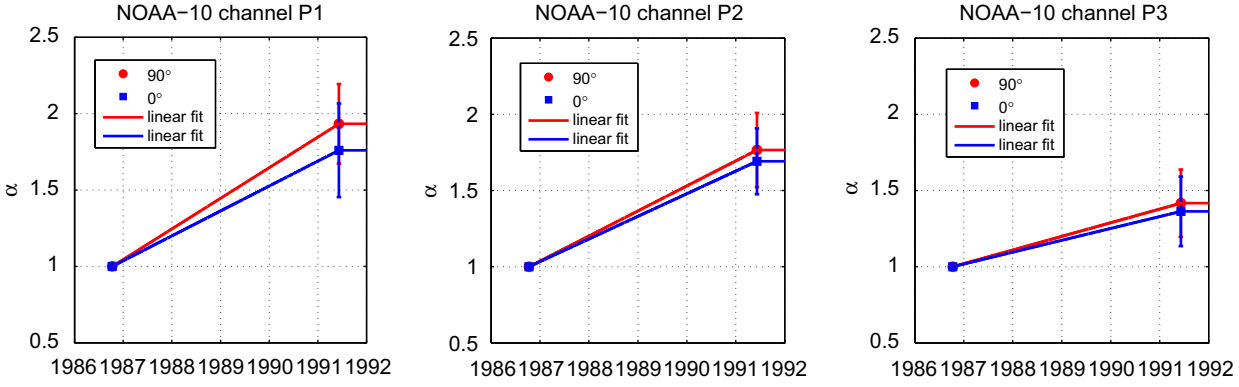

Fig. 5. The α factors of NOAA-10 as a function of time for the three lowest energy channels. The blue (black in grayscale) squares depict the 0° channel and the red (gray in grayscale) circles the 90° channel. The α factors are based on conjunctions between NOAA-10 and NOAA-12. (For interpretation of the references to color in this figure legend, the reader is referred to the web version of this article.)

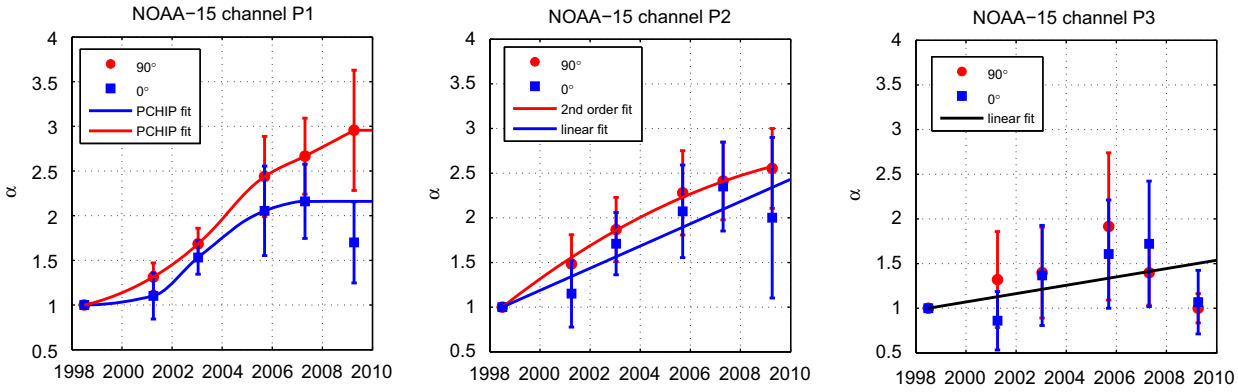

Fig. 7. The α factors of NOAA-15 as a function of time for the three lowest energy channels. The blue (black in grayscale) squares depict the 0° channel and the red (gray in grayscale) circles the 90° channel. The α factors are based on conjunctions between NOAA-15 and NOAA-16, NOAA-17, NOAA-18, METOP-02 and NOAA-19. (For interpretation of the references to color in this figure legend, the reader is referred to the web version of this article.)

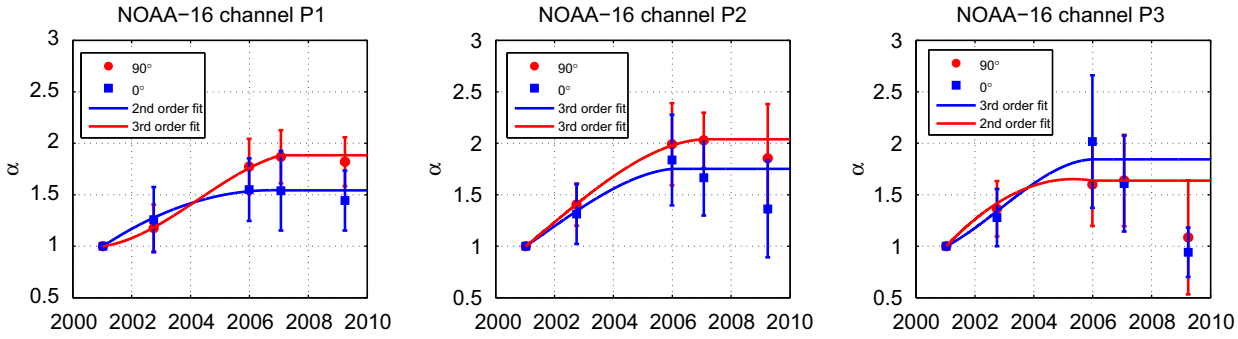

Fig. 8. The α factors of NOAA-16 as a function of time for the three lowest energy channels. The blue (black in grayscale) squares depict the 0° channel and the red (gray in grayscale) circles the 90° channel. The α factors are based on conjunctions between NOAA-16 and NOAA-17, NOAA-18, METOP-02 and NOAA-19. (For interpretation of the references to color in this figure legend, the reader is referred to the web version of this article.)

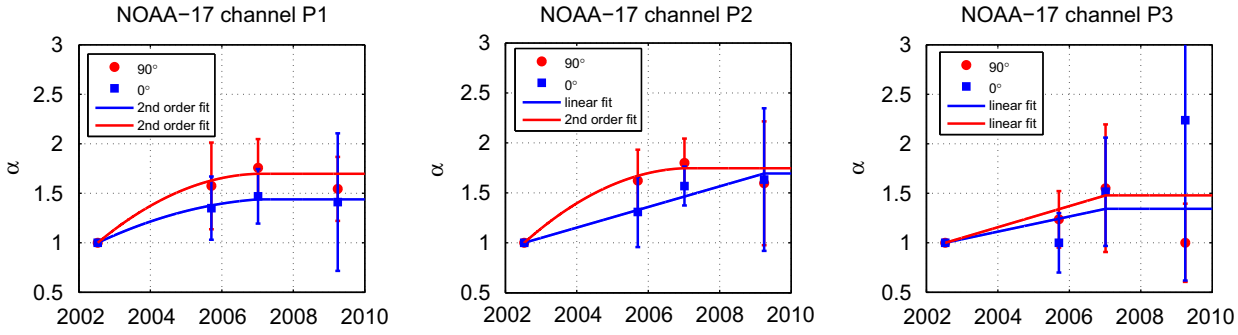

Fig. 9. The α factors of NOAA-17 as a function of time for the three lowest energy channels. The blue (black in grayscale) squares depict the 0° channel and the red (gray in grayscale) circles the 90° channel. The α factors are based on conjunctions between NOAA-17 and NOAA-18, METOP-02 and NOAA-19. (For interpretation of the references to color in this figure legend, the reader is referred to the web version of this article.)

during conjunctions. The situation with NOAA-12 was further complicated by sporadic data gaps at the end of NOAA-12 dataset. In Figs. 4–11 the blue (black in grayscale) squares depict the 0° channel and the red (gray in grayscale) circles the 90° channel. The curves represent suitable fits (either multilinear, polynomial or PCHIP) to the measured data. In each case the fitting method was chosen by visually inspecting the behavior of α factors. In cases where only one α could be determined linear fitting was used. In most other cases a 2nd or 3rd order polynomial fit described well the behavior of α in time. In the case of P1 (0° and 90°) channels of NOAA-15 the behavior of α could not be well described by a simple polynomial (while maintaining the monotonicity of the α development). In these cases the PCHIP interpolation was used. Tables 4–7 display the numerical α factors for 0° and 90° detectors at three lowest energy channels for all the satellites. The displayed α factors were computed from the fits shown in Figs. 4–11 at the midpoints of each year of satellite operation. All the α–factors for a given satellite are 1.0 at the launch of the satellite (see Table 1 for the launch times). In our calculations the fits have been used to compute the daily α–factors which were then used to recalibrate the data of each satellite. Using a constant α value for a one day of data does not produce a significant error but speeds up the calculations. From the figures one can clearly see that the energy thresholds mostly increase as a function of time and the thresholds begin to deviate significantly from the nominal value typically 2–3 years after satellite launch. We note that similar cross-calibrations as done here (but concerning mainly the lowest energy channel and the SEM-2 satellites, e.g., not as extensive study as here) has been performed at the NOAA by D. Evans (for more information see the

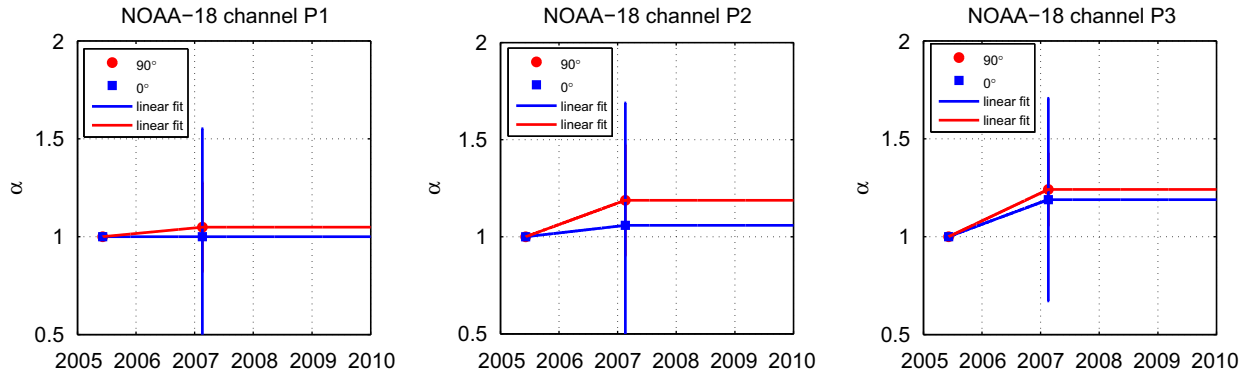

Fig. 10. The α factors of NOAA-18 as a function of time for the three lowest energy channels. The blue (black in grayscale) squares depict the 0° channel and the red (gray in grayscale) circles the 90° channel. The α factors are based on conjunctions between NOAA-18 and METOP-02. (For interpretation of the references to color in this figure legend, the reader is referred to the web version of this article.)

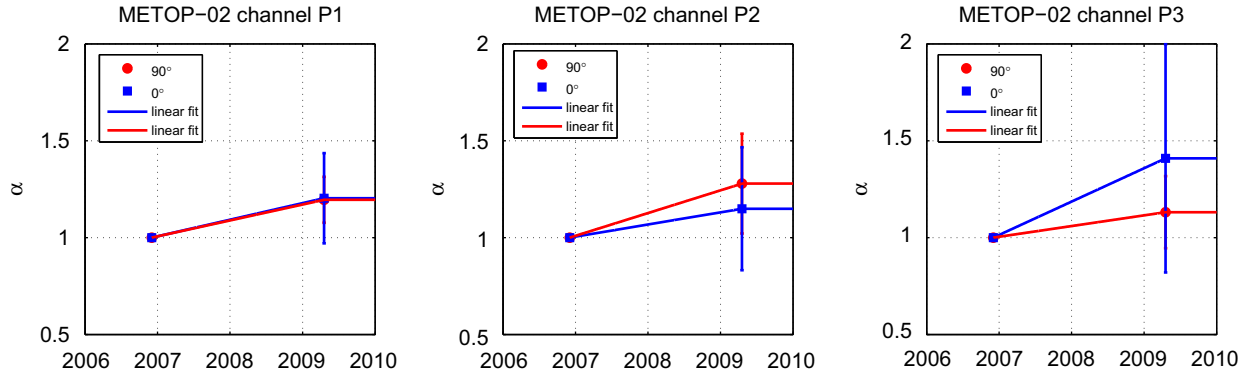

Fig. 11. The α factors of METOP-02 as a function of time for the three lowest energy channels. The blue (black in grayscale) squares depict the 0° channel and the red (gray in grayscale) circles the 90° channel. The α factors are based on conjunctions between METOP-02 and NOAA-19. (For interpretation of the references to color in this figure legend, the reader is referred to the web version of this article.)

Table 4
Tabulated α−factors for the 0° proton channel of NOAA-06, NOAA-10 and NOAA-12 for mid point of each year.

α−factors for 0° proton channels					
Year	NOAA-06	Year	NOAA-10	Year	NOAA-12
1980	[1.08; 1.12; 1.12]	1987	[1.12; 1.11; 1.06]	1991	1.01
1981	[1.16; 1.25; 1.23]	1988	[1.28; 1.26; 1.13]	1992	1.16
1982	[1.23; 1.37; 1.35]	1989	[1.44; 1.40; 1.21]	1993	1.32
1983	[1.31; 1.49; 1.46]	1990	[1.61; 1.55; 1.29]	1994	1.47
1984	[1.39; 1.62; 1.58]	1991	[1.77; 1.70; 1.37]	1995	1.62
1985	[1.47; 1.74; 1.69]			1996	1.77
1986	[1.55; 1.86; 1.81]			1997	1.92
				1998	2.07
				1999	2.22
				2000	2.37
				2001	2.37
				2002	2.37

Each column contains the α−factors for the three lowest energy channels respectively ($[\alpha_1;\alpha_2;\alpha_3]$), except for NOAA-12 where the single reported α−value applies for all the three channels. Note that at the launch of a satellite (see Table 1) the α−factors are 1.0 for the given satellite.

Table 5
Tabulated α−factors for the 90° proton channel NOAA-06, NOAA-10 and NOAA-12 for mid point of each year.

α−factors for 90° proton channels					
Year	NOAA-06	Year	NOAA-10	Year	NOAA-12
1980	[1.08; 1.13; 1.10]	1987	[1.15; 1.12; 1.06]	1991	1.01
1981	[1.15; 1.27; 1.20]	1988	[1.35; 1.28; 1.15]	1992	1.16
1982	[1.23; 1.40; 1.30]	1989	[1.55; 1.45; 1.24]	1993	1.31
1983	[1.31; 1.53; 1.40]	1990	[1.75; 1.61; 1.33]	1994	1.45
1984	[1.38; 1.67; 1.50]	1991	[1.95; 1.78; 1.42]	1995	1.60
1985	[1.46; 1.80; 1.60]			1996	1.75
1986	[1.53; 1.93; 1.69]			1997	1.90
				1998	2.04
				1999	2.19
				2000	2.34
				2001	2.34
				2002	2.34

Each column contains the α−factors for the three lowest energy channels, respectively ($[\alpha_1;\alpha_2;\alpha_3]$), except for NOAA-12 where the single reported α−value applies for all the three channels. Note that at the launch of a satellite (see Table 1) the α−factors are 1.0 for the given satellite.

instrument status reports at NOAA/POES website http://www.ngdc.noaa.gov/stp/NOAA/noaa_poes.html and Section 4.3.3 in McFadden et al., 2007). The estimated increases in the proton detector energy thresholds in that work closely resemble the results given here.

The time evolution of the α−factors differs between the satellites, between the different sensors and energy channels. This is expected since the MEPED degradation depends on the cumulative count rate measured by each instrument. The count rates are different for different satellites mainly due to the different phasing with solar activity cycle and the different satellite orbits. Within one satellite the α−factors of P3 channel are mostly lower than those of P1 and P2 channels. This is also expected since the degradation of different energy channels is expected to be caused mainly by the particles that the channel measures. Particles of different energies are stopped at different

Table 6
Tabulated α−factors for the 0° proton channel of NOAA-15, 16, 17, 18 and METOP-02 for mid point of each year.

α−factors for 0° proton channels					
Year	NOAA-15	NOAA-16	NOAA-17	NOAA-18	METOP-02
1998	[1.00; 1.00; 1.00]				
1999	[1.02; 1.12; 1.05]				
2000	[1.06; 1.25; 1.09]				
2001	[1.13; 1.37; 1.14]	[1.09; 1.09; 1.08]			
2002	[1.39; 1.50; 1.19]	[1.24; 1.29; 1.28]			
2003	[1.64; 1.62; 1.23]	[1.36; 1.48; 1.51]	[1.15; 1.10; 1.07]		
2004	[1.86; 1.75; 1.28]	[1.44; 1.63; 1.70]	[1.27; 1.20; 1.15]		
2005	[2.03; 1.87; 1.33]	[1.49; 1.73; 1.82]	[1.36; 1.31; 1.23]	[1.00; 1.00; 1.01]	
2006	[2.13; 2.00; 1.37]	[1.50; 1.76; 1.83]	[1.42; 1.41; 1.30]	[1.00; 1.04; 1.12]	
2007	[2.16; 2.12; 1.42]	[1.54; 1.76; 1.84]	[1.44; 1.51; 1.34]	[1.00; 1.06; 1.19]	[1.05; 1.04; 1.10]
2008	[2.16; 2.24; 1.47]	[1.54; 1.76; 1.84]	[1.44; 1.62; 1.34]	[1.00; 1.06; 1.19]	[1.14; 1.10; 1.27]
2009	[2.16; 2.37; 1.51]	[1.54; 1.76; 1.84]	[1.44; 1.69; 1.34]	[1.00; 1.06; 1.19]	[1.20; 1.15; 1.41]

Each column contains the α−factors for the three lowest energy channels respectively ($[\alpha_1; \alpha_2; \alpha_3]$), except for NOAA-12 where the single reported α−value applies for all the three channels. Note that at the launch of a satellite (see Table 1) the α−factors are 1.0 for the given satellite.

Table 7
Tabulated α−factors for the 90° proton channel of NOAA-15, 16, 17, 18 and METOP-02 for mid point of each year.

α−factors for 90° proton channels					
Year	NOAA-15	NOAA-16	NOAA-17	NOAA-18	METOP-02
1998	[1.00; 1.00; 1.00]				
1999	[1.08; 1.21; 1.05]				
2000	[1.20; 1.41; 1.09]				
2001	[1.35; 1.60; 1.14]	[1.03; 1.11; 1.14]			
2002	[1.56; 1.77; 1.19]	[1.14; 1.35; 1.37]			
2003	[1.81; 1.93; 1.23]	[1.31; 1.58; 1.53]	[1.26; 1.28; 1.10]		
2004	[2.12; 2.08; 1.28]	[1.50; 1.77; 1.63]	[1.47; 1.50; 1.21]		
2005	[2.40; 2.21; 1.33]	[1.68; 1.92; 1.65]	[1.61; 1.65; 1.32]	[1.00; 1.01; 1.01]	
2006	[2.56; 2.32; 1.37]	[1.82; 2.02; 1.65]	[1.68; 1.73; 1.42]	[1.03; 1.12; 1.15]	
2007	[2.69; 2.43; 1.42]	[1.88; 2.04; 1.65]	[1.70; 1.75; 1.49]	[1.05; 1.19; 1.24]	[1.05; 1.07; 1.03]
2008	[2.84; 2.52; 1.47]	[1.88; 2.04; 1.65]	[1.70; 1.75; 1.49]	[1.05; 1.19; 1.24]	[1.13; 1.19; 1.09]
2009	[2.99; 2.59; 1.51]	[1.88; 2.04; 1.65]	[1.70; 1.75; 1.49]	[1.05; 1.19; 1.24]	[1.20; 1.29; 1.13]

Each column contains the α−factors for the three lowest energy channels, respectively ($[\alpha_1; \alpha_2; \alpha_3]$), except for NOAA-12 where the single reported α−value applies for all the three channels. Note that at the launch of a satellite (see Table 1) the α−factors are 1.0 for the given satellite.

depths in the detector and produce damage in the silicon lattice at different depths. Thus the mobility of free charges in the detector depends on the depth (and energy of the incoming particle). Since there are less of higher energy particles than lower energy particles the α−factors are expected to be lower at higher energy channels.

Interestingly most α−factors in NOAA-15, 16 and 17 seem to stop increasing and even start decreasing after 2006–2007. This is probably related to the exceptionally weak solar activity in the late declining phase of solar cycle 23 when the occurrence rate of magnetic storms and high particle fluxes is reduced. The decrease in some α−factors at this time suggests that the MEPED detectors may begin to anneal after the radiating particle fluxes are reduced. The process of annealing is a well known property of solid state silicon detectors that occurs spontaneously when irradiation of the detector decreases (Grupen and Shwartz, 2008). However, the decrease in the α factors is mostly based on the α factors determined by NOAA-19 conjunctions in 2009 which are statistically very unreliable (even though the MAD values are relatively small, the α histograms do not show a clear distribution) especially in the P3 channels. Furthermore, since the errors in the α−factors from 2006 onwards do not rule out perhaps a more reasonable scenario where the rate of degradation just drops close to zero, we have set the α−factors to a constant level after they have reached their maximum or after the last conjunction. An exception to this was made in the case of NOAA-06 where we only have one determined α−factor in the early phase of the satellites life-time. In this case we extrapolated the linear trend of the α−factors until the end of the mission in 1986. This extrapolation decreases the discontinuity in the flux levels between NOAA-06 and subsequent NOAA-10.

6. The corrected measurements

Figs. 12 and 13 show the monthly averaged corrected (thick lines) and uncorrected (thin lines, except for NOAA-07 which has been plotted in thick line for clarity) fluxes of 0° (Fig. 12) and 90° (Fig. 13) detectors at three lowest energy channels. The top three panels in both figures show the P1 fluxes computed by (a) linear extrapolation, (b) by Maxwellian extrapolation and (c) as a logarithmic average of linear and Maxwellian extrapolations (i.e., taking the average of the logarithmic values). The two bottom panels show the fluxes of P2 and P3 energy channels corrected with PCHIP interpolation as explained above. The different satellites are color coded as indicated in the figure legend. (Note that NOAA-19 has not yet been included in the plots due to its short data span of only three months at the time of writing, and that NOAA-12 data after 1 May 2000 has been removed from the plots in Fig. 13 since the data of 90° channels is corrupted after that time). The whole set of data covers nearly continuously over 30 years from 1979–2009 with the exception of a 7 month data gap in 5 March–11 October 1986 in NOAA-06 and a 7 month data gap in 1 March–30 September 1988 in NOAA-10.

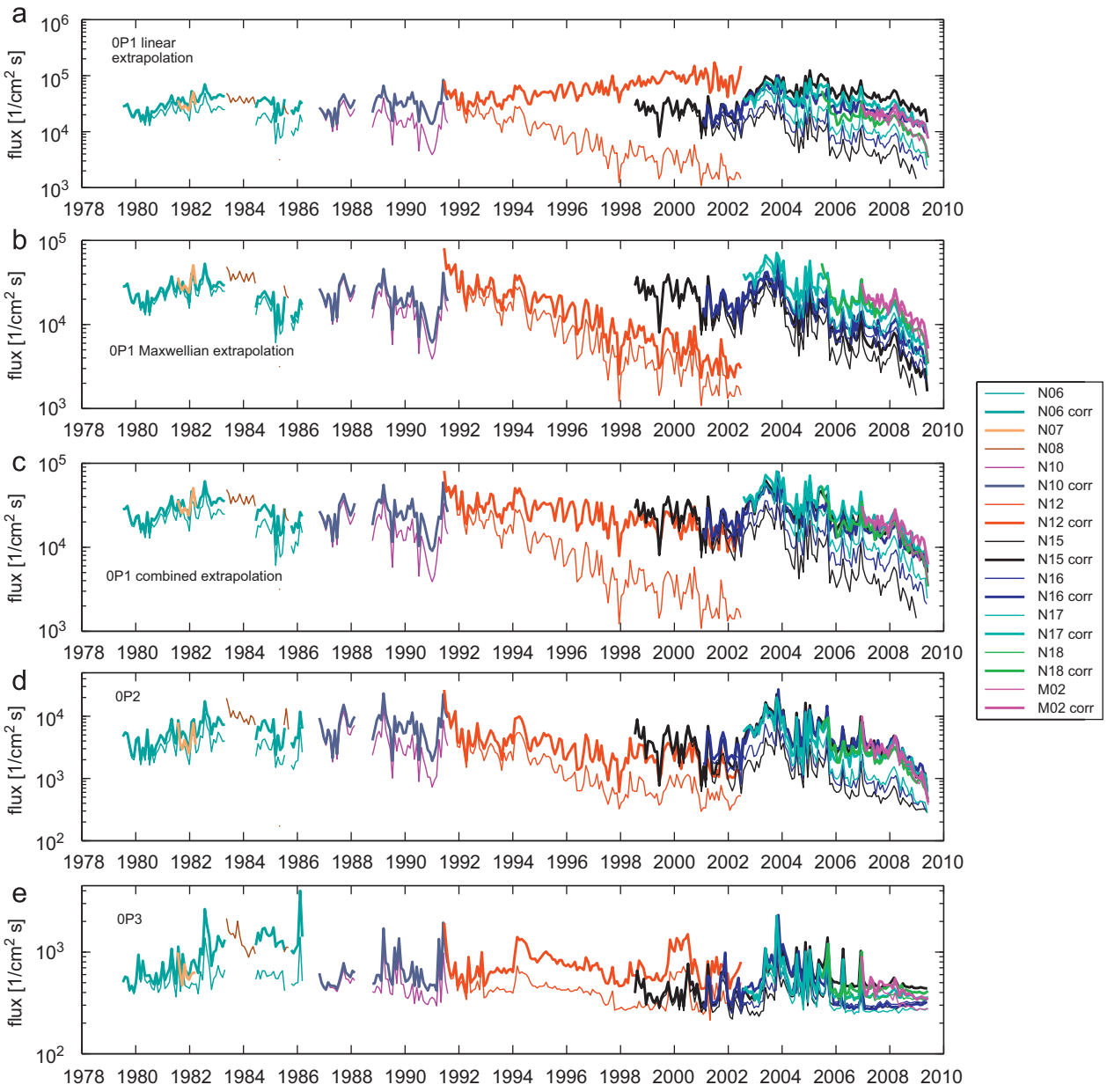

Fig. 12. Corrected (thick lines) and uncorrected (thin lines) 0° proton fluxes for P1-P3 channels. Panels from top to bottom are (a) P1 fluxes computed by linear extrapolation, (b) P1 fluxes computed by Maxwellian extrapolation, (c) P1 fluxes as a logarithmic average of linear and Maxwellian extrapolations, (d) P2 fluxes, and (e) P3 fluxes.

Examining the uncorrected fluxes shows that the fluxes indeed decrease over long periods of time due to radiation damage. This is especially evident in the case of NOAA-12 and NOAA-15 that have the longest series of measurements spanning over 10 years each. Comparing corrected and uncorrected fluxes shows that the radiation damage begins to affect the fluxes noticeably about 2–3 years after satellite launch. The effect of this damage is most evident during the overlapping time intervals of different satellites, and causes a significant disagreement between the uncorrected flux levels measured by an old satellite and a new one. On the other hand, the flux levels are considerably more similar after the correction. This improvement is especially visible in all the depicted panels in late 1991 between NOAA-10 and NOAA-12. Note that these satellites have the same orbital plane and are thus expected to see very similar flux levels. The agreement between two overlapping satellites is improved in all cases after the present correction of fluxes.

Accordingly, the corrected fluxes presented here present a great improvement but some deficiencies still remain. The most important problem in our method is related to the extrapolation of the measured spectrum to obtain the corrected flux for the lowest P1 energy channel. The error related to extrapolation is expected to grow with α, which is corroborated by the three top panels in Figs. 12 and 13. The top panel shows that the linear extrapolation method tends to overestimate the flux considerably. This is clear when comparing NOAA-12 with NOAA-15 in 1999. The flux levels of the two satellites should be very similar due to their nearly identical orbital planes. However, the linear correction exaggerates the NOAA-12 flux greatly. Similarly the linearly corrected fluxes of NOAA-15, NOAA-16 and NOAA-17 tend to be overestimated and are rather different already in 2004 and onwards.

The Maxwellian extrapolation method in contrast tends to underestimate the fluxes, as can be seen from the discontinuity

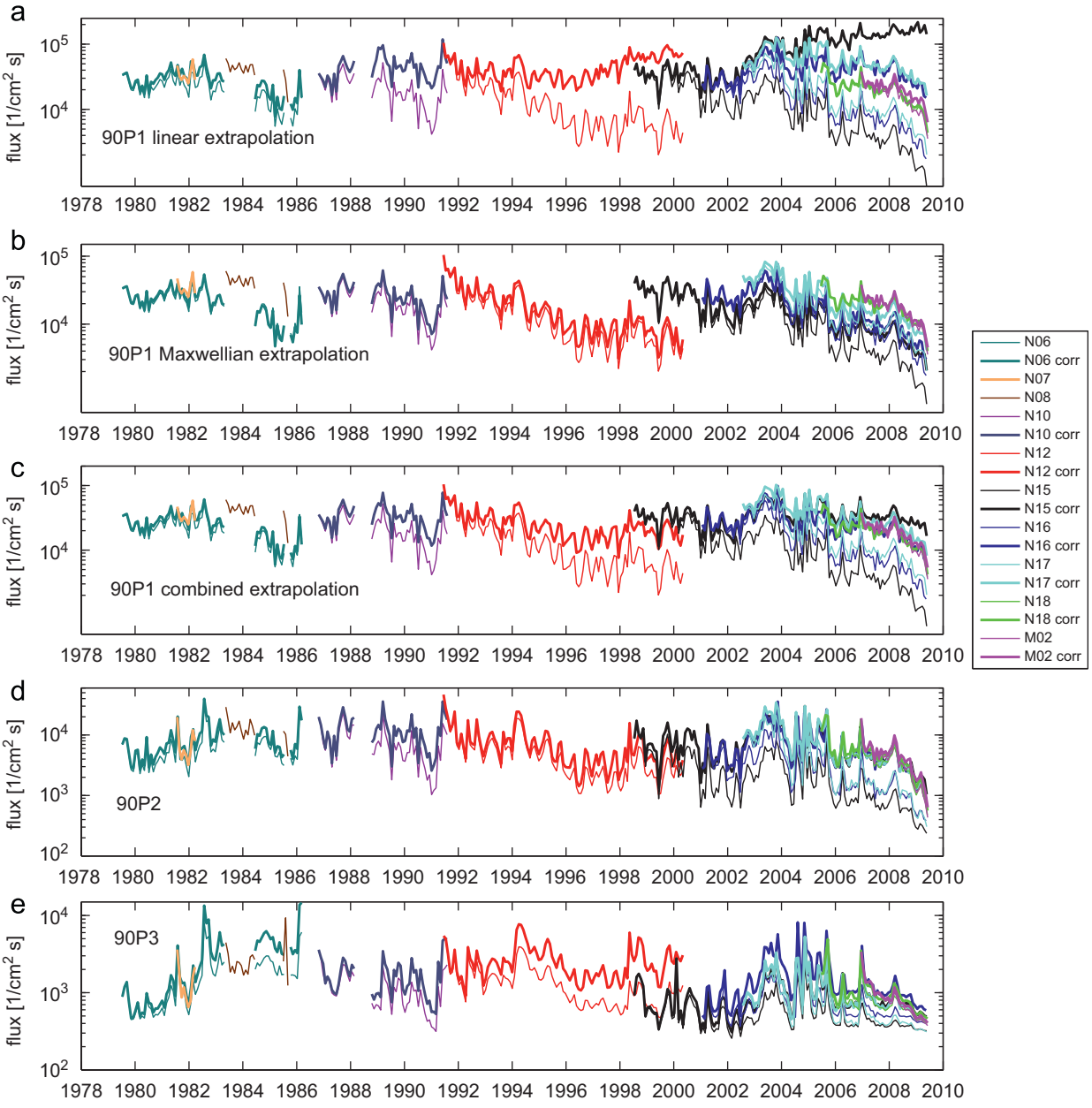

Fig. 13. Corrected (thick lines) and uncorrected (thin lines) 90° proton fluxes for P1-P3 channels. Panels from top to bottom are (a) P1 fluxes computed by linear extrapolation, (b) P1 fluxes computed by Maxwellian extrapolation, (c) P1 fluxes as a logarithmic average of linear and Maxwellian extrapolations, (d) P2 fluxes, (e) P3 fluxes. Note that NOAA-12 data after 1 May 2000 has been removed from these plots since the data of 90° channels is corrupted after that time.

between NOAA-10 and NOAA-12 in 1991 and NOAA-12 and NOAA-15 in 1999 (Figs. 12b and 13b). The same underestimation is evident in the Maxwellian corrected fluxes of NOAA-15, 16 and 17 after 2006 when compared to the newly launched NOAA-18 and METOP-02 satellites. It seems that on an average, the energy spectrum is somewhat curved downwards between the P1 and P2 channels (30–80 keV) which would explain the overestimation when using linear extrapolation and underestimation when using extrapolating using a Maxwellian spectrum which flattens out rather quickly towards lower energies. So, as a compromise between these two methods we also computed the logarithmic average of the fluxes corrected by the two different extrapolation methods. The result of this is shown in the third panel (c) of Figs. 12 and 13. One can see that this method improves the agreement between P1 flux levels of two overlapping satellites especially in the end of NOAA-12, NOAA-15, NOAA-16 and NOAA-17 data sets.

Let us next consider some sources of error in our recalibration method. When determining the α factors we select conjunction times up to 5 month after the launch of the new satellite, i.e., we assume that during the first 5 month from the launch the instruments of the new satellite are not degraded (in fact, on an average the conjunctions take place about 2.5 month after the launch of a new satellite). While some radiation damage does occur to the new satellite during these 5 month it has a very small effect on the determined α factors. This can be seen from the determined α factors in Figs. 4–11. In each satellite the α factors change only slightly during the first 5 month. Furthermore we cannot see any significant difference in the uncorrected and corrected fluxes in any satellite during the first 5 month of the satellites life time (see Figs. 12 and 13). (Note that the same is true when looking at the fluxes in 2 s resolution.) Another possible source of error might be contamination of the proton detector by relativistic electrons. However, this contamination occurs only in

the P6 channel which has been left out of the analysis precisely for this reason.

The uncertainty of the α factors lead to a time dependent uncertainty in the corrected count rates. The effect of the α error $\Delta\alpha$ on the corrected count rates may roughly be estimated by assuming that the spectrum is locally power law (i.e., a line in log–log scale) between two energy channels. It is fairly straight forward to show that the relative error of the corrected count rates at channel i is approximately given by

$$\frac{\Delta N_{c,i}}{N_{c,i}} = (\gamma - 1)\frac{\Delta\alpha_i}{\alpha_i}, \tag{14}$$

where γ is the spectral index between energies $\alpha_i E_i$ and $\alpha_{i+1}E_{i+1}$. On an average the relative error of the α factors from all satellites and energy channels is about 0.2 (20%) and the long-term average spectral index is around $\gamma = 2.5$. These values give an estimated average relative error of about 30% due to the uncertainty in the α values.

As discussed above, the corrected fluxes at the lowest energy channel show obvious systematic error. It can be seen in Figs. 12 and 13 that the correction of the P1 channel gives poor results especially when the energy threshold has increased significantly over a factor of about 1.5. The average overestimation of the linear extrapolation method and the average underestimation of the Maxwellian extrapolation show that the spectrum is on average slightly curved downwards between the P1 and P2 energy channels. This suggests that it might be possible to estimate this spectral curvature using undegraded data and use that information to produce a better correction. Furthermore, it is likely that the measured energy specta show systematic curvature (either upward or downward) also on higher energies which in turn may lead to systematic errors in the corrected fluxes of P2, P3, P4 and P5 channels. Again, studying the average shape of the spectra may give additional information which could be used to improve the corrected fluxes of all the channels, however, such a study is beyond the scope of the work presented here. Visual examination of the flux levels in Figs. 12 and 13 suggests that the order of magnitude of the relative systematic error of P1 channel can at worst be around $+50\%$. The systematic error of P2 and P3 channels seems to be much less and probably not very significant. Finally, we wish to note that the correction method presented here is, of course, not the only method that can be used to correct the count rates, but an example of a simple general method that works fairly well, especially for P2 and P3 channels, regardless of spectral shape. In some particular cases where the spectral shape is more accurately known, a better fit than PCHIP might be obtained for the spectrum, resulting in a more accurate correction. However, for an automated correction of a large amount of data, regardless of spectral shape, interpolating the observed spectrum by PCHIP or by some other method, instead of fitting some specific mathematical form, is probably the only possibility.

7. Conclusions

In this paper we have presented a systematic method for estimating the level of radiation damage on MEPED proton detectors and a possible method for recalibrating the measured MEPED proton fluxes for all the NOAA/POES satellites. This method is based on a physical model of radiation damage where the effective energy thresholds of the instrument increase as the radiation damage progresses. The calculation of the corrected count rates of the different energy channels presented here requires either interpolation or extrapolation to the nominal energy thresholds on the basis of measured data on the elevated energy thresholds. The results of the applied correction shown here indicate that the correction on those energy channels where interpolation is performed, i.e., P2 and P3 (and P4 and P5 that are not shown here), yields rather good results. This can be seen as an improved continuity between the data from two consecutive satellites and a lower difference between the overall flux levels of overlapping data from different satellites. In contrast, for the lowest energy channel, where extrapolation to lower energies than measured by the satellite is required, the correction gives less accurate results especially when the energy threshold has increased by a factor of larger than about 1.5. In cases where the spectral shape is definitely known, more accurate results may be obtained by fitting a more specific mathematical form to the spectrum than a polynomial interpolant.

We have applied our method of correction to over 30 years of energetic particle data to produce for the first time a database that takes fairly reliably into account the long-term effects of the radiation damage to the instruments. We have systematically quantified the degree of radiation damage on all the NOAA/POES MEPED proton detectors and produced the α factors describing the increases in the individual energy thresholds of the instrument channels. Such knowledge is of great importance to the long-term studies of the Sun–Earth connection and Earth's magnetosphere as it allows us to more reliably study the long-term changes in the magnetospheric energetic particle fluxes as well as their connection to geomagnetic and solar activity.

Acknowledgments

We wish to thank Dr. David Evans at NOAA for his help and useful discussions on the MEPED instruments. The research leading to these results has received funding from the European Commission's Seventh Framework Program (FP7/2007-2013) under the Grant agreement no. 218816 (SOTERIA project, www.soteria-space.eu). We also acknowledge the financial support by the Academy of Finland to the HISSI research project no. 128189.

References

Asikainen, T., Kerttula, R., Mursula, K., Friedel, R., Baker, D., Søraas, F., Fennell, J., Blake, J., 2005. Global view of energetic particles during a major magnetic storm. In: Pulkkinen, T., Tsyganenko, N., Friedel, R. (Eds.), The Inner Magnetosphere: Physics and Modeling of Geophysical Monograph, Vol. 155. American Geophysical Union, pp. 97–104.

Asikainen, T., Mursula, K., 2005. Filling of the South Atlantic Anomaly by energetic electrons during a great magnetic storm. Geophys. Res. Lett. 32 (L16102 doi:10.1029/2005GL023634.

Asikainen, T., Mursula, K., 2008. Energetic electron flux behavior at low L-shells and its relation to the South Atlantic Anomaly. J. Atmos. Solar-Terrestrial Phys. 70, 532–538.

Evans, D.S., Greer, M.S., 2000. Polar orbiting environmental satellite space environment monitor—2: instrument descriptions and archive data documentation. NOAA Technical Memorandum, Boulder, Colorado OAR SEC-93.

Fritsch, F.N., Carlson, R.E., 1980. Monotone Piecewise Cubic Interpolation. SIAM J. Numer. Anal. 17, 238–246.

Fung, S., 1996. Recent development in the NASA trapped radiation models. In: Lemaire, J., Heynderickx, D., Baker, D. (Eds.), Radiation Belts: Models and Standards of Geophysical Monograph, Vol. 97. American Geophysical Union, pp. 79–91.

Galand, M., Evans, D., 2000. Radiation damage of the proton MEPED detector on POES (TIROS/NOAA) satellites. NOAA Technical Memorandum, Boulder, Colorado OAR 456-SEC 42.

Grupen, C., Shwartz, B., 2008. Particle Detectors of Cambridge Monographs on Particle Physics, Nuclear Physics and Cosmology, vol. 26, second ed. Cambridge University Press.

Hill, V.J., Evans, D.S., Sauer, H.H., 1985. TIROS-N/NOAA satellites space environment monitor archive tape documentation. NOAA Technical Memorandum, Boulder, Colorado ERL SEL-71.

Huston, S., Kuck, G., Pfitzer, K., 1996. Low altitude trapped radiation model using TIROS/NOAA data. In: Lemaire, J., Heynderickx, D., Baker, D. (Eds.), Radiation belts: Models and Standards of Geophysical Monograph, Vol. 97. American Geophysical Union, pp. 119–122.

McFadden, J., Evans, D., Kasprzak, W., et al., 2007. In-flight instrument calibration and performance verification. In: Wüest, M., Evans, D.S., von Steiger, R. (Eds.),

Calibration of Particle Instruments in Space Physics. Vol. SR-007 of ISSI Scientific Report, ESA Publications Division, pp. 277–385.

Raben, V.J., Evans, D.S., Sauer, H. H., Sahm, S.R., Huynh, M., 1995. TIROS/NOAA satellite space environment monitor data archive documentation: 1995 update. NOAA Technical Memorandum, Boulder, Colorado ERL SEL-86.

Seale, R.A., Bushnell, R.H., 1987. The TIROS-N/NOAA A-J space environment monitor subsystem. NOAA Technical Memorandum, Boulder, Colorado ERL SEL-75.

Søraas, F., Aarsnes, K., Oksavik, K., 2002. Ring current intensity estimated from low-altitude proton observations. J. Geophys. Res. 107 (A7 doi:10.1029/2001JA000123.

Søraas, F., Aarsnes, K., Oksavik, K., Sandanger, M., Evans, D., Greer, M., 2004. Evidence for particle injection as the cause of Dst reduction during HILDCAA events. J. Atmos. Solar-Terrestrial Phys. 66, 177–186.

Wissing, J., Bornebusch, J., Kallenrode, M.-B., 2008. Variation of energetic particle precipitation with local magnetic time. Adv. Space Res. 41, 1274–1278.